On the post-impact fatigue behavior and theoretical life prediction of CF/PEEK-titanium hybrid laminates using an energy dissipation approach

Ji, Chunming; Hu, Jiqiang; Alderliesten, René; Yang, Jinchuan; Zhou, Zhengong; Sun, Yuguo; Wang, Bing

Important note
To cite this publication, please use the final published version (if applicable).
Please check the document version above.

On the post-impact fatigue behavior and theoretical life prediction of CF/PEEK-titanium hybrid laminates using an energy dissipation approach

Chunming Ji [a,b], Jiqiang Hu [a], René Alderliesten [b], Jinchuan Yang [a], Zhengong Zhou [a], Yuguo Sun [a], Bing Wang [a,*]

[a] National Key Laboratory of Science and Technology on Advanced Composites in Special Environments, Harbin Institute of Technology, Harbin, 150001, PR China
[b] Structural Integrity & Composites Group, Faculty of Aerospace Engineering, Delft University of Technology, Kluyverweg 1, 2629 HS, Delft, the Netherlands

ABSTRACT

This paper aims to illustrate the effect of the impact damage on fatigue behavior of CF/PEEK-titanium hybrid laminates. To achieve this end, a fatigue life model was proposed to predict the S–N curves of the laminates at various initial impact energy levels and stress ratios based on the energy dissipation approach. The energy dissipation behavior of the laminates during fatigue loading under different experimental conditions was analyzed through a large amount of post-impact fatigue tests, and the correlation between the initial impact damage and the total fatigue dissipation energy was determined. The full-field axial strain distribution of the titanium layer on the impacted side of the laminate was characterized in terms of initial impact energy level and maximum stress using digital image correlation, and then the post-impact fatigue failure mechanism of CF/PEEK-Ti hybrid laminates was summarized. Finally, the validity of the proposed model was verified by fatigue tests under other conditions of stress ratio and impact energy level. It is worth mentioning that the proposed model is also applicable to other types of FMLs, and can accurately predict the residual fatigue life of laminates after impact with only one set of S–N curve data.

1. Introduction

Due to the coexistence of metal and fiber reinforced polymer composites, the fiber metal laminates (FMLs) perform excellent resistance to fatigue and impact in a proper stacking sequence [1–5]. Compared with conventional metals, FMLs have a wide prospect of application in the transportation fields with lightweight needs, such as aerospace and automobile [6,7]. In particular, the second generation of FMLs, called glass fiber reinforced epoxy composite/aluminum (GLARE) laminates, have been commercially applied in the upper fuselage skin panel of Airbus A380 [8]. However, due to the limited temperature resistance of aluminum alloy and epoxy resin, employing GLARE laminates in an elevated temperature environment (nearly 177 °C for the surface temperature of supersonic vehicles [9]) is impossible. Therefore, titanium-based FMLs were developed, where the adoption of titanium prevents the electrochemical corrosion issues between the stronger carbon fibers and aluminum alloys [10,11], enabling the application of carbon fibers in FMLs. Coupled with the use of high-temperature resistant resins (such as PEEK/PPS), titanium-based FMLs are expected to

serve for a long duration in elevated temperature environments, making them one of the important materials of choice for the next generation of supersonic aircraft.

Various defects and damages are often unintentionally introduced into aircraft structures during manufacturing and service, severe damage conditions can degrade the fatigue resistance of the material, leading to a reduction in service life and an increase in the probability of failure [12]. In particular, foreign object damage (FOD) including low-velocity impact is one of the frequent forms of structural damage to aircraft [13–15], such as dropping tools, runway debris and hailstones. For metallic materials, the fatigue behavior [16–18] and residual strength [19–21] after low-velocity impact with various types of inserts, and the fatigue behavior after dent repairing [22,23] have been extensively investigated. However, for composite materials, especially the research on post-impact fatigue performance of FMLs is limited, and most of the available results focus on experimental studies [2,24,25]. Compared with fiber-reinforced polymer composite laminates, impact damage on the surface of FMLs is more readily detected visually. Nonetheless, damage such as fiber breakage, matrix cracks, and

delamination inside the laminates due to low-velocity impact cannot be inspected visually, and such damage may lead to a substantial decrease in the fatigue life of the composites [26]. Therefore, evaluating the effect of initial impact damage on the residual fatigue life of the laminates and the corresponding failure mechanism are essential for the engineering application and minimizing the maintenance cost of FMLs.

Fatigue life prediction methodologies for composites can be generally classified into three categories [27]: fatigue life models based on experimental data (S–N curves, machine learning, etc.) [28,29], phenomenological models (residual strength/stiffness models) [30–32], and progressive damage models [33,34]. However, the damage mechanism in FMLs after impact is remarkably complex, and the prediction using S–N curves or machine learning requires a considerable amount of experiments and is usually dependent on the type of material; the residual strength/stiffness model is unable to explain the deformation of FMLs throughout the entire fatigue course; while the progressive damage model needs to introduce a series of damage and property degradation criteria of material when applied to the post-impact fatigue issue, which makes the model extremely complicated. To avoid analyzing the complex damage mechanisms during post-impact fatigue, predicting the residual fatigue life of FMLs after impact from an energy perspective is an effective approach. Movahedi-Rad et al. [35] used an energy dissipation approach to predict the cyclic-creep life of viscoelastic materials, and the proposed model can yield an acceptable life prediction of the tensile-tensile fatigue at various stress ratios, including stress ratio close to 1 where the creep effect is significant. Li et al. [36] established a model for predicting the fatigue limit and S–N curves of short carbon fiber reinforced PEEK based on the laws of thermodynamics and the fatigue damage mechanism by analyzing the intrinsic source of energy dissipation during fatigue, and the prediction results were in good agreement with the experiments.

In the present work, regarding the typical service condition of post-impact fatigue in engineering applications, a fatigue life model was proposed to predict the S–N curves of CF/PEEK-Ti hybrid laminates under different initial impact energy levels and stress ratios based on the method of energy dissipation. Then, through a large amount of post-impact fatigue tests, the energy dissipation behavior of CF/PEEK-Ti hybrid laminates under different experimental conditions was analyzed, and the correlation between the initial impact damage and the total dissipated energy in fatigue was determined. Besides, the full-field axial strain distribution of the titanium layer on the impacted side of the laminate was characterized in terms of initial impact energy level and maximum stress using digital image correlation, and the post-impact fatigue failure mechanism of CF/PEEK-Ti hybrid laminates was summarized. Finally, the validity of the proposed model was verified by fatigue tests under other conditions of stress ratio and impact energy level.

2. Experimental method and results

2.1. Materials and preparation

The material used for investigating the post-impact fatigue behavior is CF/PEEK-titanium hybrid laminates, the main components include the commercially pure titanium sheet with a thickness of 0.3 mm (Baoji titanium industry Co. Ltd.), the unidirectional prepreg of CETEX TC1200 with a thickness of 0.13 mm (TenCate Co. Ltd.) that consists of AS-4 carbon fibers and PEEK (59% in fiber volume fraction), and the PEEK film with a thickness of 0.1 mm (Victrex plc.) that used to provide a basic interfacial adhesion between the titanium and CF/PEEK layers. Besides, the interfaces between titanium and the CF/PEEK layers were further strengthened using sandblasting and electrophoretically deposited network structure of multi-walled carbon nanotubes (MWCNTs) as described in Ref. [37]. The deposition treatment of titanium layers could provide a better interfacial behavior of the laminates under both quasi-static and dynamic out-of-plane loading [37,38] compared to

sandblasted-only treatment, where the deposition time is 90 s and the MWCNTs concentration is 0.75 mg/mL. After the pretreatment of titanium surface, the hot-pressing method was adopted to prepare the hybrid laminates with a cross-ply stacking sequence of Ti/[0/0/90/90]/Ti/[90/90/0/0]/Ti in the customized frame mold, the hot-pressing parameters and process can be found in Ref. [38].

2.2. Experimental methods and characterization

The impact tests were performed on a drop-weight testing machine (CEAST 9350, Instron) as illustrated in Fig. 1(a). A hemispherical insert with a diameter of 16 mm was adopted for the impact which was perpendicular to the surface of the laminate, and the impact energy levels were selected as 5, 10, 15 and 20 J (corresponding to velocities of 1.35, 1.91, 2.34 and 2.70 m/s, respectively), therein, the impact energy level of 10 J corresponds to the energy generated by a wrench of about 800 g falling at a height of 1.25 m. Due to limited research addressing the issue of post-impact fatigue in FMLs, there is no clear standard for the geometry of the specimen used in fatigue testing. It has been reported that the dog-bone specimens were used in post-impact fatigue testing of composites, but this type of specimen was prone to fracture at the transition region rather than the weak part (dent) of the test region [24,39]. To prevent the residual fatigue life of the impacted specimens from being underestimated, in combination with the fatigue-related test standard for metallic materials (ASTM E466) and resin matrix composites (ASTM D3479/D3039), and considering the requirement of a sufficiently large area for the low-velocity impact test to minimize the boundary effect, a rectangular specimen was employed for the subsequent fatigue test of the CF/PEEK hybrid laminates, the dimension of the specimen was designed to be 75 mm × 200 mm as illustrated in Fig. 1(c), where the impact position is located at the center of the specimen.

The post-impact fatigue tests were carried out using a servo-hydraulic testing machine (322.41, MTS) in a force-controlled method as shown in Fig. 1(b). The loading waveform is sinusoidal and the frequency is 3Hz (to prevent the specimen from degradation of materials due to the overheating induced by the internal friction). The whole course of fatigue was simultaneously coupled with the digital image correlation (DIC) technique for measuring the surface strain on the impacted side of the specimen, and a complete waveform was collected once every 500 cycles. The principal factors affecting the fatigue life of FMLs include stress ratio, maximum stress, layup sequence, level of impact damage, and other environmental variables. In this study, the layup sequence and the interface strengthening method remained invariant, and the post-impact fatigue behavior of CF/PEEK-Ti hybrid laminates was investigated under various maximum stresses. The maximum stress level R_σ is defined as the ratio of the maximum stress σ_{max} during fatigue to the tensile strength of the laminate σ_t, as characterized in Eq. (1). The maximum stress levels were selected as 20%, 30%, 40% and 50% (corresponding to maximum stresses of 146.66, 219.98, 293.31 and 366.64 MPa, respectively), the stress ratio was set as 0.1, and the geometry of the tab is illustrated in Fig. 1(c). Based on the conditions of the post-impact fatigue, the specimens were labeled as *E-R_σ*, where *E* and *R_σ* refer to the impact energy level (0, 5, 10, 15, or 20 J) and the maximum stress level (20%, 30%, 40%, or 50%), respectively. Fatigue tests were conducted up to 10^6 cycles or up to the complete fracture of the laminate, and three samples for each impact and fatigue condition were tested. The failure morphology on the hybrid laminate was analyzed by using a scanning electron microscope (SU8010, Hitachi) operated at 10 kV, and the cross-sectional fracture morphology was examined by using a stereomicroscope (SZ61, Olympus).

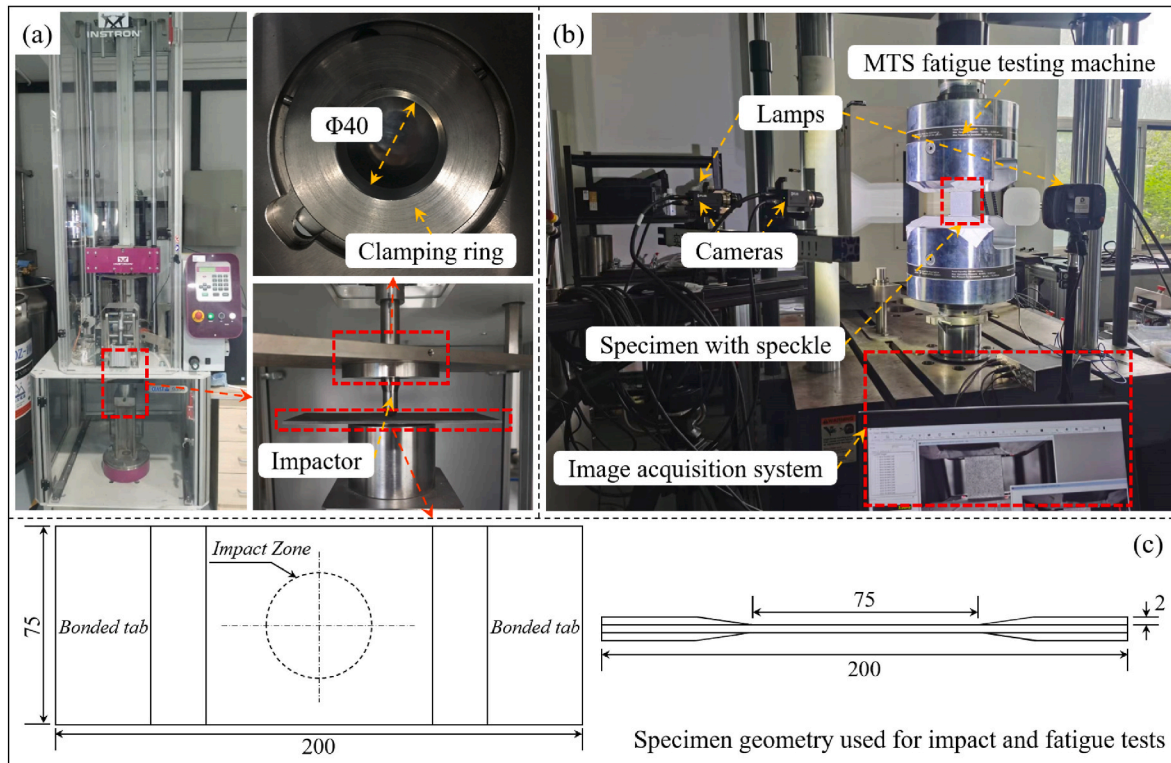$$R_\sigma = \frac{\sigma_{max}}{\sigma_t} \tag{1}$$

Fig. 1. Experimental set-up of (a) impact and (b) fatigue tests; (c) specimen geometry used for impact and fatigue tests.

3. Experimental results and discussion

3.1. Post-impact fatigue life distribution

Fig. 2 presents the residual fatigue life distribution (in logarithmic representation) under different maximum stresses of the laminates with initial impact damage. Regarding the same initial impact energy level, the residual fatigue life of the specimens exhibited a significant decreasing trend with the increase of the maximum stress during fatigue. Under the same magnitude of cyclic stress, the higher the initial impact energy level of the specimens, the lower the residual fatigue life. For the cases with lower maximum stress level (20% of tensile strength), the residual fatigue life of the specimens exceeded 10^6 cycles for all but 20 J
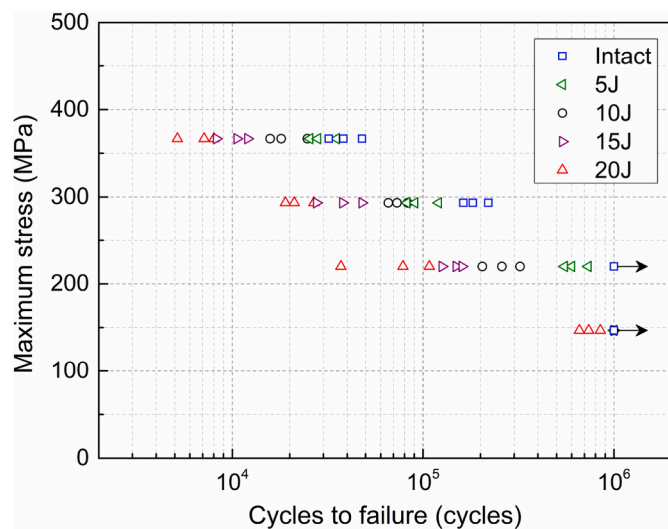

Fig. 2. Residual fatigue life distribution of the specimens with initial impact damage under different maximum stress levels.

of impact energy level. At the maximum stress level of 50%, the average residual fatigue life of the laminate with the initial impact energy level of 20 J decreases to 17.2% of the fatigue life of the intact specimen.

Fatigue crack initiation life is critical for evaluating the integrity of the material over its service period. To acquire the fatigue crack initiation life of the laminate, virtual extensometers from DIC analysis were set up at the center, left side and right side (at the strain peaks) of the dent to measure the variation of axial strain around the dent (Fig. 3(a)), and the collected axial strain in the entire period of fatigue is shown in the schematic diagram of Fig. 3(b), which includes cycle acquisition (data of a complete waveform) and peak acquisition (data of peak and valley). A crack is considered to have appeared at the location when there is a sudden increase in axial strain (E1, the center of the dent) as shown in Fig. 3(b), which avoids the situation where the location and time of crack appearance cannot be accurately determined by the naked eyes. The average fatigue cycle distribution for different experimental conditions when the crack appears on the impacted side (fatigue crack initiation life) is presented in Fig. 3(c), for all specimens with pre-impact damage, cracks first emerged from the center or both sides of the dent in the titanium layer on the impact side, while for intact specimens, cracks appeared from the edge of the specimen with a random initiation location. The fatigue cycles to crack initiation gradually decreased as the impact energy level and the maximum stress increased. At the maximum stress level of 50% and the impact energy level of 20 J, the average number of cycles to crack initiation decreased to 17% of that of the intact specimens, which is close to the percentage reduction of the residual fatigue life.

3.2. Full-field strain analysis

Full-field strain nephogram is one of the most intuitive ways to monitor the fatigue crack propagation and damage evolution of FMLs [40]. Fig. 4 illustrates the axial strain evolution of intact specimen during fatigue loading with the maximum stress of 293.31 MPa (40% of tensile strength), using a stationary legend and sorted by different
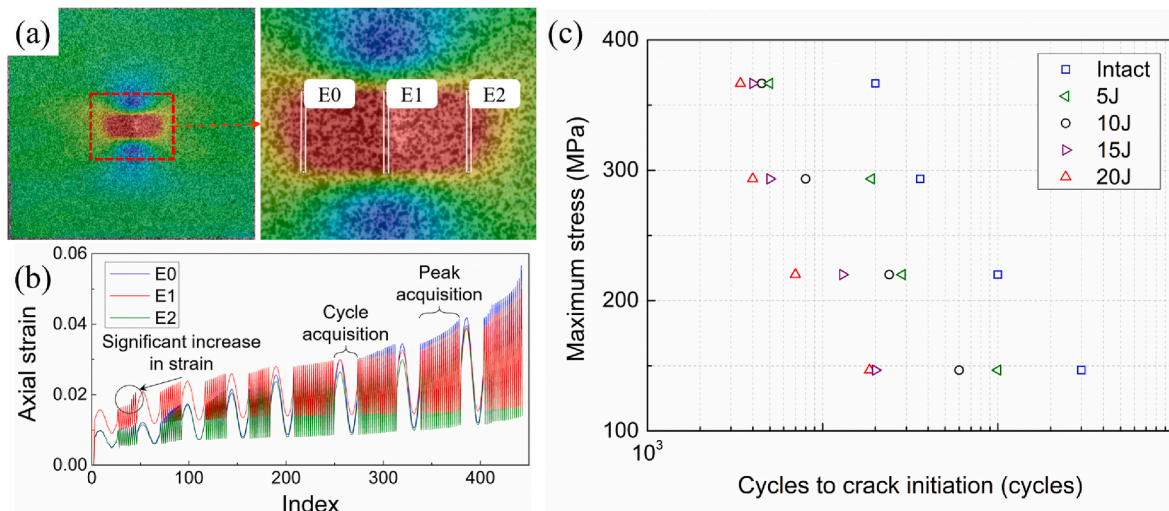
Fig. 3. (a) Position of the virtual extensometers; (b) schematic diagram for acquiring the axial strain; (c) average fatigue cycles distribution when the crack appears on the impacted side.
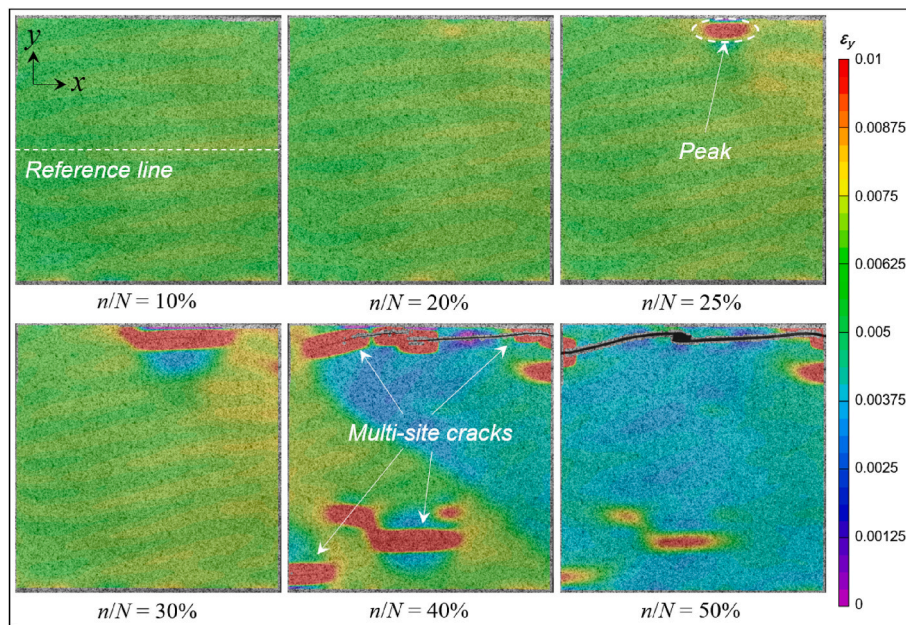

Fig. 4. Axial strain evolution of intact specimen during fatigue loading with the maximum stress of 293.31 MPa.

fatigue cycle ratios n/N, where n and N are the experienced fatigue cycles and the total fatigue life, respectively. In the preliminary stage of the fatigue life of the intact specimen ($n/N = 10\%$), the axial strain distribution on the surface of the specimen is uniform, and there is no obvious area with stress concentration. As the experienced fatigue cycle increases, the fatigue cracks gradually initiate in the outer titanium layer and are distributed in the form of multiple points ($n/N = 40\%$), which eventually triggers the complete fracture of the outer titanium layer. For FMLs, it is indicated that the outer metal layer is not subjected to applied loading if the axial strain is 0, which means that the metal layer is delaminated from the internal composite layer. For the intact specimens at the stage of n/N less than 50%, the axial strains on the outer titanium layer are greater than 0 at almost all positions, which demonstrated that there is no delamination between the outer titanium layer and the internal CF/PEEK layer, implying that the specimen has an excellent interfacial property.

For the specimens with initial impact damage, taking 15J-40% as an

example, compared to the intact specimen (Fig. 4), the axial strain on the impacted-side surface of the titanium layer is redistributed due to the presence of the dent as shown in Fig. 5, and the stress is concentrated at the center of the dent ($n/N = 10\%$). With the increase in the experienced fatigue cycles, fatigue cracks also initiated at the center of the dent ($n/N = 30\%$). Besides, the outer titanium layer is still not completely fractured when the experienced fatigue cycles reach 90% of the total fatigue life, while for the intact specimen (Fig. 4), the outer titanium layer is fully fractured when the experienced fatigue cycles equal to 50% of the total fatigue life, which indicates that the internal CF/PEEK layer remains capable of withstanding a large number of fatigue cycles for the intact cases, but for the impacted specimens, the fatigue life of the internal CF/PEEK layer is significantly degraded by the impact damage, which reduces the residual fatigue life of the whole laminate.

A straight line is marked along the fracture path of the specimen with impact dent and the same location (reference line) of the intact specimen as illustrated in Figs. 4 and 5, the axial strain distribution history at the
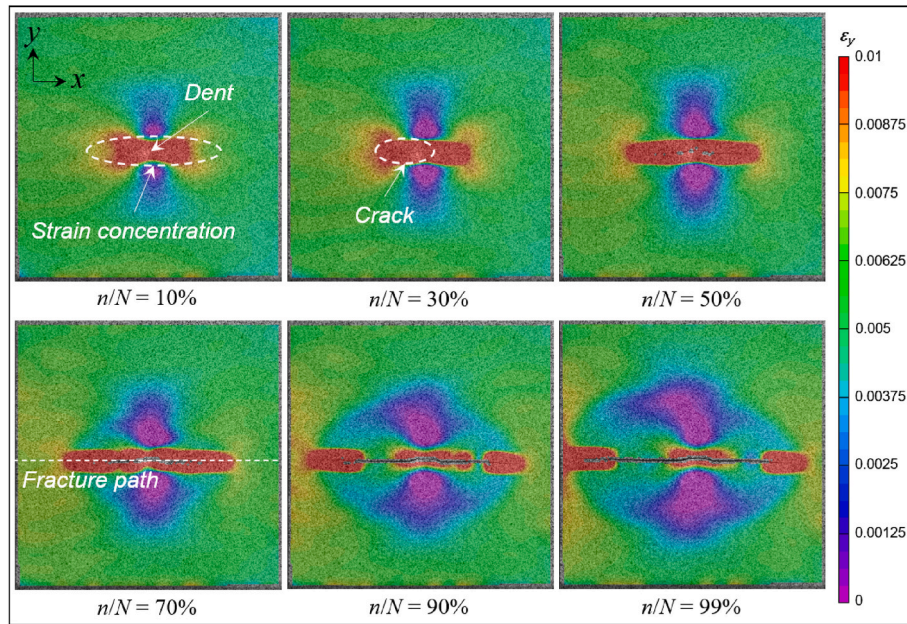
Fig. 5. Axial strain evolution of dented specimen (15 J) during fatigue loading with maximum stress level of 293.31 MPa.

straight line is acquired by DIC post-processing analysis for comparison. Fig. 6(a) and (b) show the axial strain history distributions along the fracture path at the maximum stress of 293.31 MPa for the intact specimen and specimen subjected to the initial impact energy level of 15 J. With increasing the experienced fatigue cycles, the axial strain along

the reference line is always uniformly distributed for intact specimens since the reference line is not the final fracture path. For the specimen with initial impact damage, the fracture path passes through the dent, and with the increase of the experienced fatigue cycles, the strain around the dent gradually increases and the cracks are initiated, then the peaks
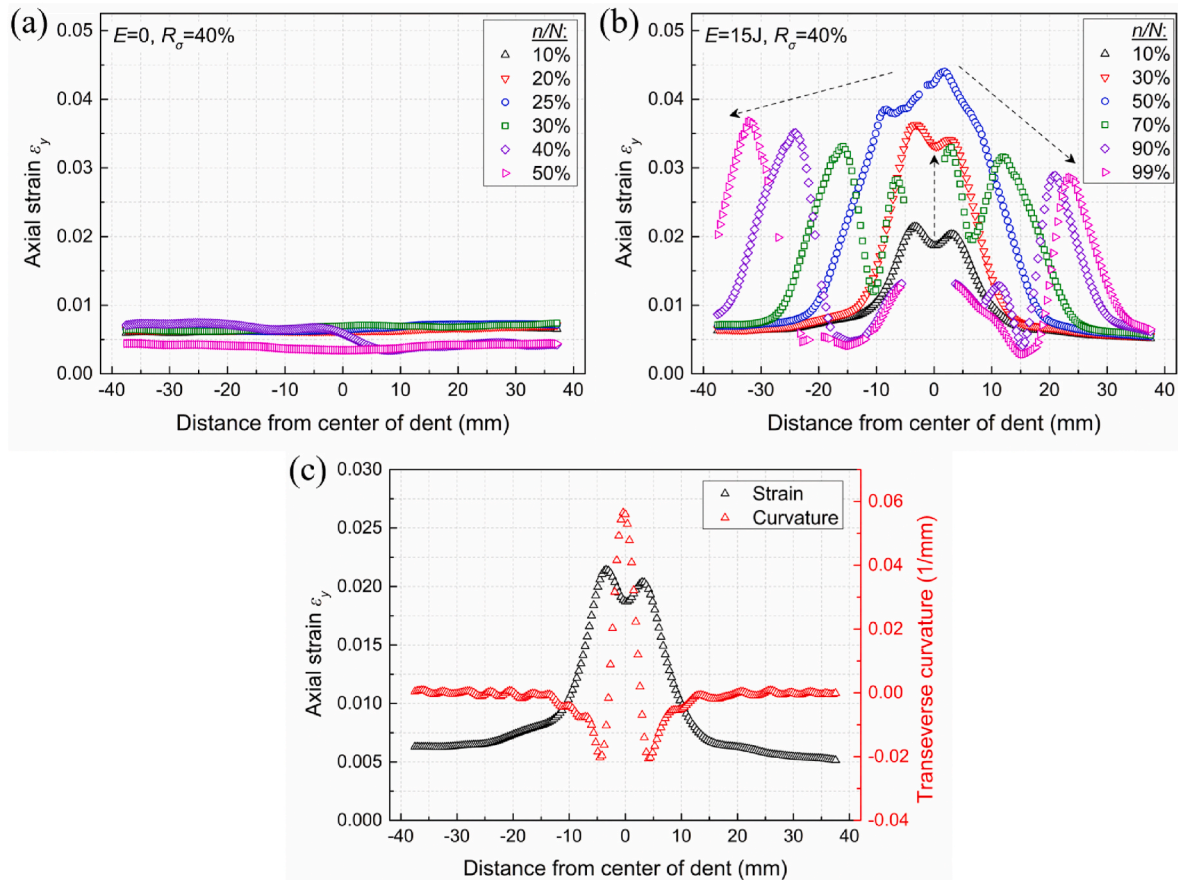

Fig. 6. Axial strain history along the reference line (the maximum stress is 293.31 MPa): (a) intact specimen; (b) specimen subjected to the initial impact energy level of 15 J; (c) comparison of axial strain (in y direction) and transverse curvature (in x direction) along the fracture path.

of axial strain on both sides of the dent expanding toward the edge of the specimen until complete fracture as presented in Fig. 6(b). In addition, similar to the result of the residual strength analysis [38], the peaks of axial strain along the fracture path of the specimen with initial impact damage are also located at the minimum transverse curvature on both sides of the dent, as shown in Fig. 6(c).

Fig. 7(a) presents the axial strain nephogram of the specimens with different impact energy levels under the maximum stress level of 50% at $n/N = 10\%$. As the initial impact energy level increases, the stress at the dent becomes more concentrated. From the corresponding axial strain history along the fracture path in Fig. 7(b), it can be seen that the peak of axial strain is located inside the dent at low impact energy levels (5 J and 10 J), when the impact energy is further increased to 15 J, the peaks of axial strain move to both sides of the dent, and the higher the impact energy level is, the farther the peaks are away from the center of the dent. Meanwhile, the axial strain at the fracture path increases gradually with the initial impact energy level, which leads to a decrease in the fatigue life of the laminates, consistent with the evolution of the fatigue life in Fig. 2. In addition, the axial strain nephogram of the specimens with the initial impact energy level of 20 J under different maximum stresses at $n/N = 10\%$ is shown in Fig. 7(c). At the maximum stress level of 20%, due to the high total fatigue life of the specimen, cracking in the outer titanium layer already appears at n/N of only 10%. From the corresponding axial strain history along the fracture path in Fig. 7(d), it can be found that for the specimen containing a 20 J impact dent, the

distance of the axial strain peaks from the center of the dent remains basically the same for different maximum stress levels, whereas for the case of $R_\sigma = 20\%$, the position of the axial strain peaks move towards the edge of the specimen compared to others, which indicates that the cracks have propagated. Similarly, for the maximum stress level of 30%, there is no shift in the position of the axial strain peaks, but cracks are visible in the nephogram, indicating that the cracks are just initiated at the stress concentration points and have not yet propagated. For the remaining maximum stress level conditions (40% and 50%), no fatigue crack initiation forms at $n/N = 10\%$ in the impacted side of the titanium layer due to the low total fatigue life of the laminates.

3.3. Fracture morphology

For all specimens with impact damage, the final fracture path passes through the dent, as shown in Fig. 8(a). Different from the fracture mode of metal materials [16], crack initiation and propagation of the outer titanium layer appear first in CF/PEEK-Ti hybrid laminates during the entire course of fatigue, even after the outer titanium layer is completely fractured, the internal carbon fiber layer still maintains well-integrity, allowing for continuing to withstand the fatigue cyclic loading and play the role of bridging mechanism without any instantaneous breakage. As illustrated in Fig. 8(b) for the lateral view of the fatigue loading course of the intact specimen and the specimen subjected to an impact energy level of 20 J. It can be observed that the edges of the
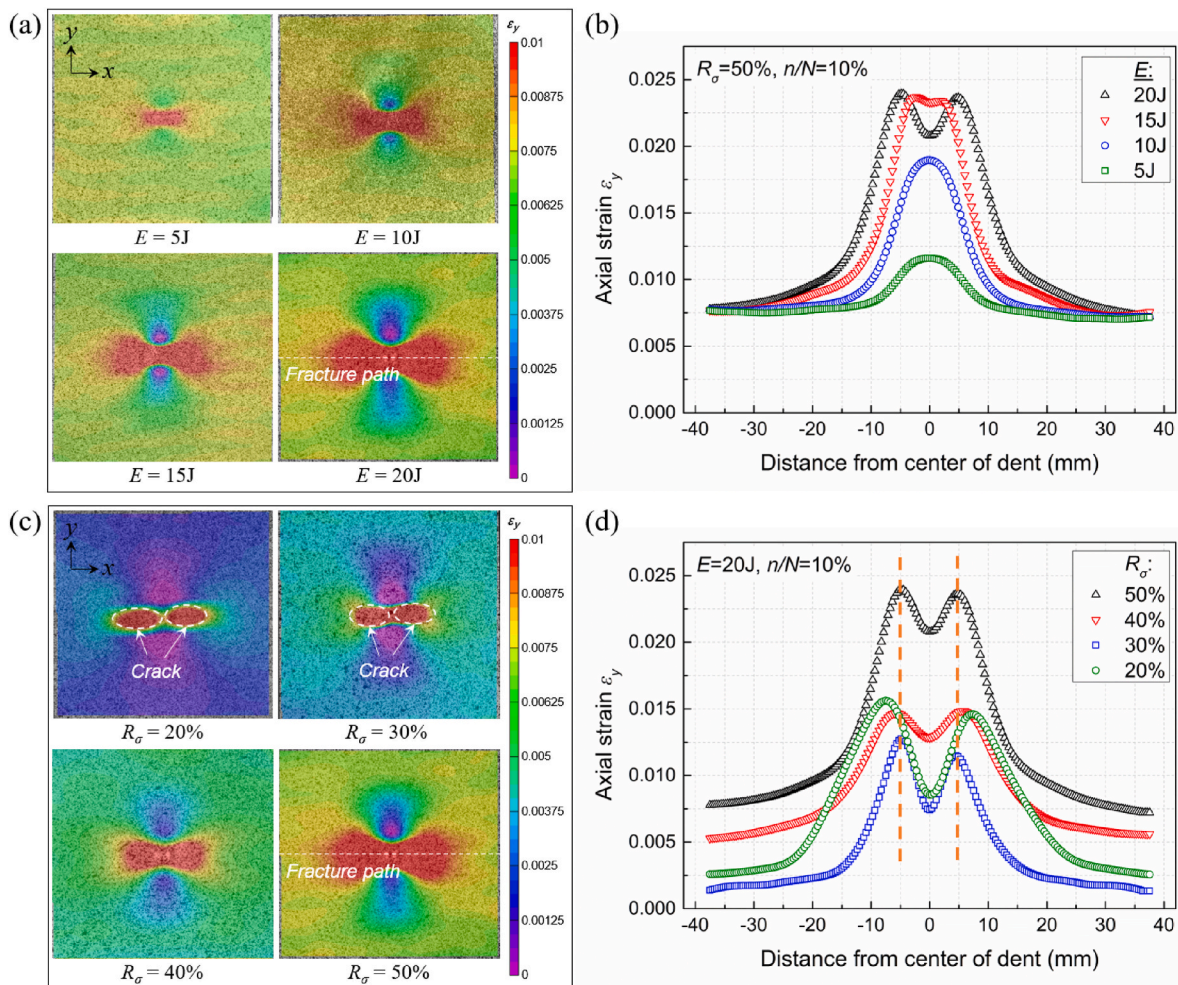

Fig. 7. For different impact energy levels under the maximum stress level of 50% at $n/N = 10\%$: (a) full-field axial strain nephogram, (b) axial strain history along the fracture path; for different maximum stresses under the impact energy level of 20 J at $n/N = 10\%$: (c) full-field axial strain nephogram, (d) axial strain history along the fracture path.
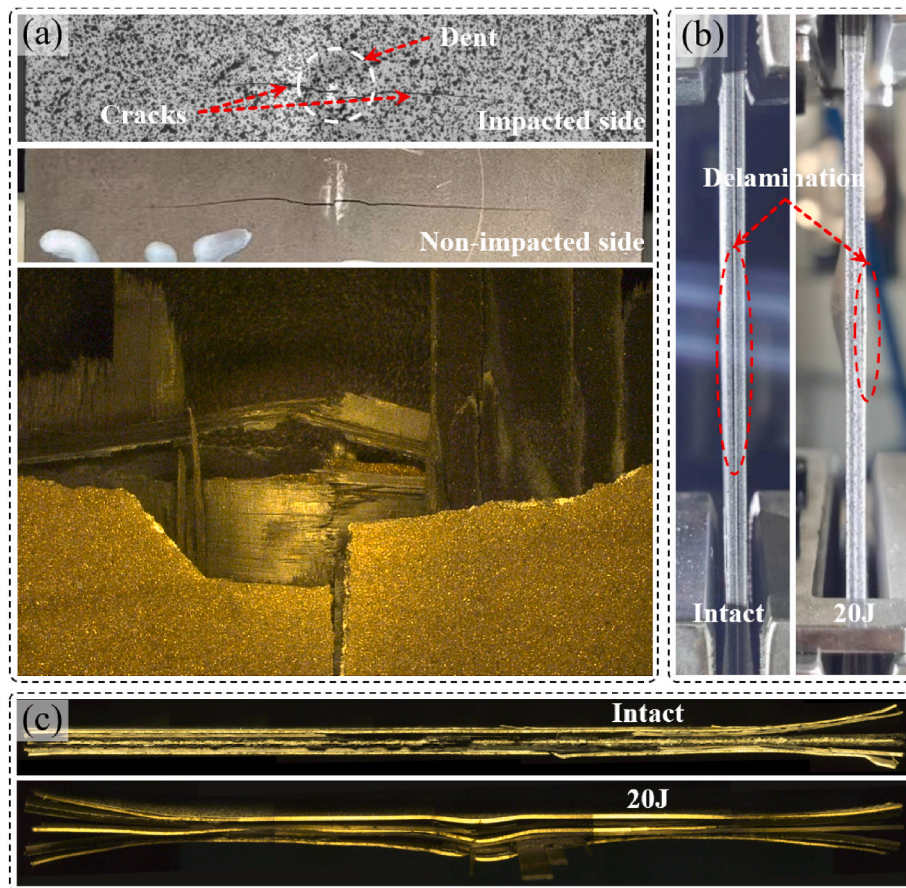
Fig. 8. (a) Local fracture morphology of the impacted side, non-impacted side and dent of the specimen subjected to an initial impact energy level of 20J; (b) lateral view of the intact specimen and the specimen subjected to an initial impact energy level of 20J during fatigue; (c) cross-sectional view of the macroscopic fracture of the intact specimen and the specimen subjected to an initial impact energy level of 20J.

intact specimen are more prone to delamination (the interface between the CF/PEEK layers and the two faces of the intermediate titanium layer), while cracks on both sides of the dent on the impacted side of outer titanium layer first appear in the specimens with initial impact damage, accompanied by delamination between the outer titanium layer on the impacted side with the neighboring CF/PEEK layer, as for the non-impacted side, only cracks are observed in the metal layer, there is no delamination around the edges.

Since the ideal curing temperature of thermoplastic resin PEEK is 380~390 °C, each component layer within the laminate after curing will be subject to an additional residual thermal stress due to the difference in coefficients of thermal expansion. Based on the analysis of the residual thermal stresses in each component layer within the laminate after impact [38], it can be found that the stresses in the outer titanium layer on the impacted side and the non-impacted side are the maximum and the minimum within the laminate under uniaxial tensile loading conditions, respectively. Therefore, the length of cracks on the impacted side of the outer titanium layer is greater than that of the non-impacted side under fatigue loading, as presented in Fig. 8(b), the impacted side of the outer titanium layer is delaminated after complete fracture, while the cracks in the non-impacted side of the outer titanium layer are still not fully connected. From the cross-section morphology of the macroscopic fracture (Fig. 8(c)), it can be seen that the specimen is delaminated only at the edges and dent under fatigue loading, and the interface of the remaining positions still maintains good bonding, indicating that there is a well-efficient stress transfer of stress transfer between the fiber and the metal layers. Comprehensively, the influence of impact dent on the residual fatigue life of FMLs can be categorized into the following aspects:

(a) Local stress concentration due to the deformation induced by the impact. Since the curvature around the dent is non-zero, a concentration of stress appears at the minimum curvature on both sides of the dent under external force, accelerating the propagation of fatigue cracks, as presented in Fig. 6;

(b) Impact leads to the delamination and fiber breakage within the laminate. As shown in Fig. 8(a), damage such as delamination between CF/PEEK and titanium layers as well as fiber breakage/ matrix cracking of CF/PEEK layer can be observed around the dent, inducing stress concentration at the tip of crack, which further decreases the post-impact fatigue life of the laminate;

(c) The residual stress field within the laminate after curing is amplified by the dent. The residual thermal stress state within each component layer of the laminate is amplified by the subjected fatigue loading and the effect of stress concentration formed by the dent geometry, resulting in more susceptibility to crack initiation (lowering the damage tolerance of the laminate) and accelerating fatigue crack propagation as well as delamination.

The microscopic morphology of the fracture within each component of the specimen (20J-40%) is shown in Fig. 9 to illustrate the energy dissipation mechanism of the laminate in microscale. It can be seen that the main failure modes of the CF/PEEK layer include tearing of the PEEK, breakage of the carbon fibers, and pull-out of the fibers due to carbon fiber/PEEK debonding (Fig. 9(a)). Although there is no visible damage on the impacted side of the outer titanium layer after impact, cracks near the dent appear first on its surface due to the effect of stress concentration (Fig. 9(b) and (c)). For the interface between titanium and
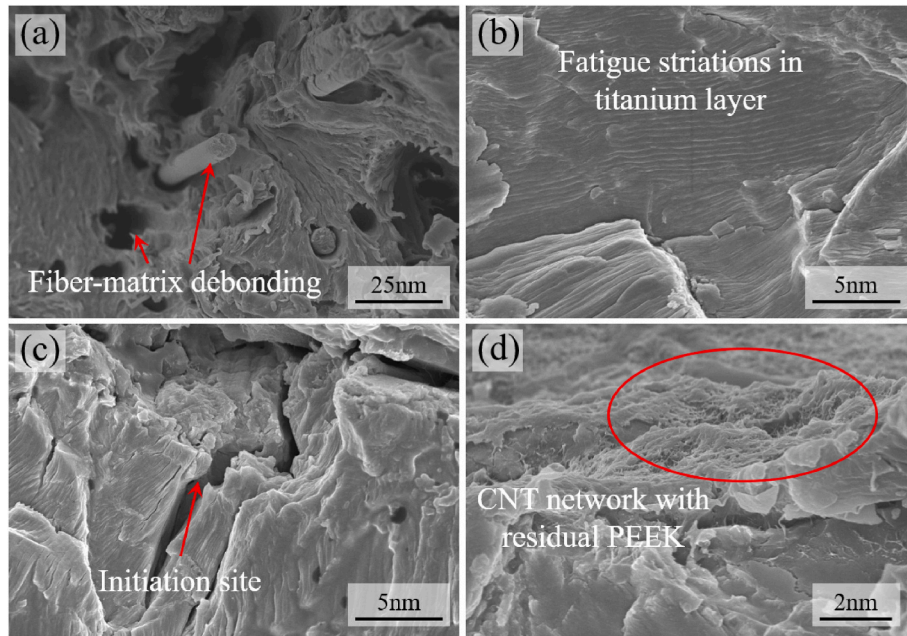
Fig. 9. Microscopic morphology of the fracture (20J-40%): (a) CF/PEEK layer; (b) inside titanium layer; (c) impacted side surface of outer titanium layer; (d) interface between titanium and CF/PEEK layers.

CF/PEEK layers as presented in Fig. 9(d), the PEEK matrix can be well locked on the surface of titanium layer by introducing the MWCNTs network structure, and the MWCNTs play the role of bridging in the interface to retard the delamination propagation, as indicated by the excellent interfacial behavior of the laminate in Fig. 8(c), which demonstrates the effectiveness of the interfacial reinforcement of the MWCNTs network structure. The energy dissipation of CF/PEEK-Ti hybrid laminates during fatigue loading, as observed from the microscopic fracture, mainly includes: (1) the initiation and propagation of micro-cracks in the titanium layers; (2) energy dissipation by the delamination between the titanium-CF/PEEK layers, the debonding of the carbon fibers-PEEK, and the pull-out of the carbon nanotubes; and (3) the breakage of carbon fibers and the cracking in PEEK. Combining the result of full-field strain analysis, the internal fiber layer is still able to withstand a high number of fatigue cycles after the fracture of the titanium layers, therefore, the dissipated energy in the early stage ($n/N<50\%$) of fatigue loading is mainly dependent on the fracture of the titanium layers and the delamination between the titanium-CF/PEEK layers.

4. Fatigue life prediction model using an energy dissipation approach

4.1. Energy-based fatigue damage accumulation analysis

Fatigue is a process with irreversible energy dissipation, the Bauschinger effect [41] leads to a hysteresis loop where the strain lags behind the stress as the material is subject to fatigue loading. Hence, the total input mechanical energy from the external source to the specimen can be characterized by the hysteresis energy density, that is, the area of the hysteresis loop, as illustrated in Fig. 10(a). In this section, the hysteresis energy densities of specimens with various initial impact damage under different maximum stress conditions were analyzed to obtain the energy dissipation behavior of post-impact fatigue, guiding the prediction of the post-impact fatigue life of CF/PEEK-Ti hybrid laminates.

The area of the hysteresis loop is related to the stress and strain histories. The hysteresis energy density increases with the stress history if only the maximum stress varies; when the stress ratio increases, the maximum stress remains constant with increasing the minimum stress during fatigue loading, then the stress history decreases, resulting in a
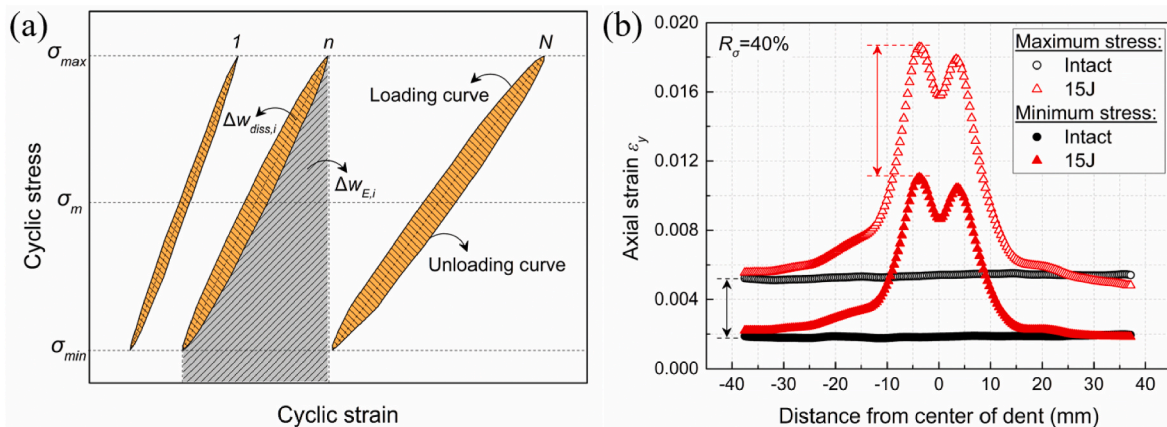

Fig. 10. (a) Schematic diagram of Bauschinger effect, (b) axial strain history of the intact specimen and the specimen with an impact dent under the same magnitude of cyclic stress.

decrease in the hysteresis energy density. In addition, with the increase of experienced fatigue cycles, damage such as cracks and delamination within the laminate leads to a decrease in stiffness, which elevates the strain history of the laminate under the same cyclic loading, resulting in an increase in the hysteresis energy density, as shown in Fig. 10(a). It can be seen from Fig. 2 that the initial impact damage has a significant effect on the residual fatigue life of the specimen. The localized stress concentration around the dent increases the strain history at the strain peak on the reference line when the specimen with initial impact damage is subjected to axial tensile loading, as illustrated in Fig. 10(b). Furthermore, impact damage such as delamination and fiber/metal fracture within the laminate reduces the stiffness of the laminate whilst increasing the strain history. Therefore, the hysteresis energy density per cycle is related to the maximum stress during fatigue loading, the stress ratio, the experienced fatigue cycles, and the degree of the initial impact damage, which is

$$\Delta w_{diss,i} = f(\sigma_{max}, n, R, E) \tag{2}$$

where, $\Delta w_{diss,i}$ is the hysteresis energy density per cycle, σ_{max}, n, R and E represent the maximum stress during fatigue loading, the experienced fatigue cycles, the stress ratio, and the initial impact energy, respectively.

For all specimens with initial impact damage, the strain measurement of the overall specimen using an extensometer could not accurately characterize the energy dissipation course locally within the specimen. As shown in Fig. 10, the strain history at the edges of the intact specimen is similar to that of the specimen subjected to impact energy of 15 J. To understand the energy dissipation course at the dent, the strain history at the peak of axial strain on both sides of the dent is used to plot the hysteresis curve. Fig. 11(a) and (b) compare the hysteresis curves at different positions of the specimen under the condition of 20J–50%, it can be seen that the hysteresis curves at the edge of the specimen (away from the dent) are different from those at the peak of strain near the dent. For the edges of the specimen, there is no significant variation in the hysteresis energy density from the beginning of fatigue to fracture,

as presented in Figs. 11(a) and 12. As for the peak of strain near the dent, the hysteresis energy density gradually increases with the experienced fatigue cycles, as indicated in Fig. 11(b), while the stiffness at the strain peak of the laminate continuously decreases, that is, a larger deformation is generated under the same cyclic loading, implying that the damage such as cracks have appeared at the position of the strain peaks (earlier fracture failure with respect to the edge of the specimen), which can also be corroborated in Fig. 3.

Comparing the hysteresis curves at the peak of strain for different impact energy levels, as illustrated in Fig. 11(c) and (d). As the initial impact energy level increases, the strain history of the hysteresis loops at 500 cycles becomes progressively larger under the same maximum stress, although the maximum stress and stress ratio are identical, the maximum strains are completely different, reaching the largest at 20 J. Similarly, for the hysteresis curves at the peak of strain near the dent at various maximum stress levels, as presented in Fig. 11(d), the stress history of the hysteresis loops gradually increases with the increase of the maximum stress level, resulting in an increase in the hysteresis energy density at this position.

It can be noticed from comparing Figs. 2 and 3 that the specimen is still able to withstand a higher number of fatigue cycles after cracking at the peaks of axial strain near the dent. Therefore, the hysteresis energy density at the edge of the specimen is used to predict the residual fatigue life of the laminate after impact. The variation law of hysteretic energy density with experienced fatigue cycles under different test conditions is shown in Fig. 12(a–e). For all test conditions, the hysteretic energy density of the specimens is capable of maintaining stability in most of the experienced fatigue cycles, and a significant and sudden jump of dissipated energy only appears near the fracture. Fig. 12(f) provides a comparison of the hysteretic energy densities of the specimens at 500 cycles for all test conditions, generally the hysteretic energy densities show an approximately linear trend of increase with increasing impact energy. At the maximum stress levels of 50% and 40% in 20J, there is a significant increase in the dissipation energy density per cycle, which is attributed to the severe damage that has appeared within the laminate (cracking in the non-impacted side of outer titanium layer, breakage of
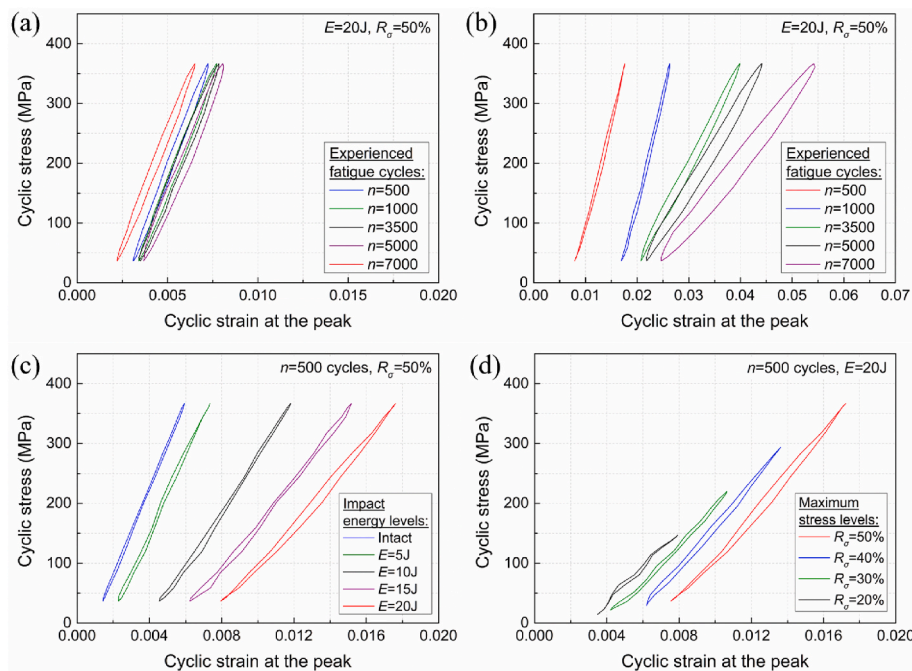

Fig. 11. Hysteresis loop curves for different experienced fatigue cycles of the specimen with an initial impact energy level of 20 J and a maximum stress level of 50%: (a) at the edge of the specimen, (b) at the strain peak near the dent; hysteresis loop curves at the strain peak near the dent for 500 experienced fatigue cycles: (c) for specimens with different initial impact energy levels at a maximum stress level of 50%; (d) for specimens with different maximum stress levels at an initial impact energy level of 20 J.
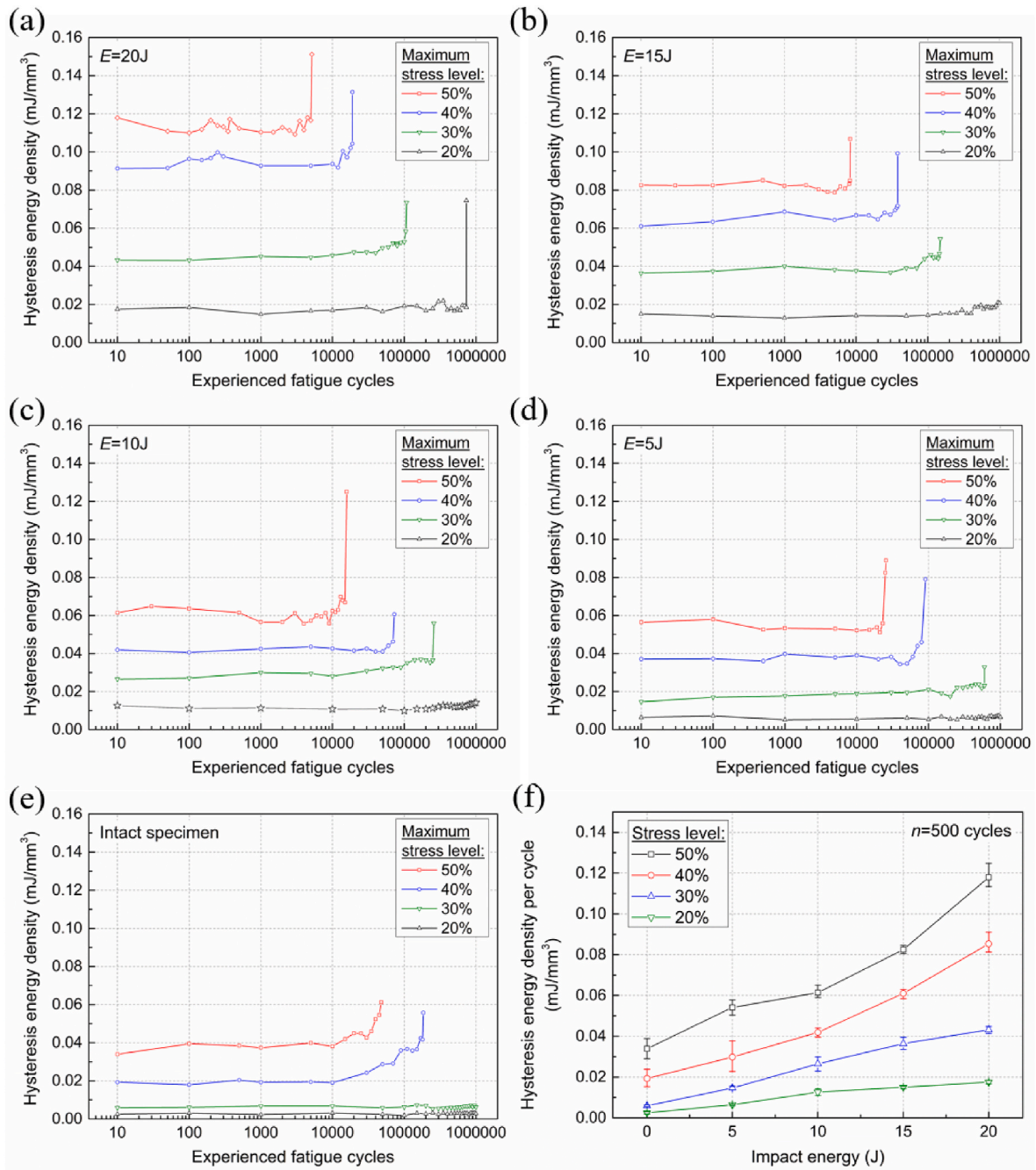
Fig. 12. Hysteresis energy densities at the edge of the specimens under different impact energy and fatigue stress levels: (a) 20J; (b) 15J; (c) 10J; (d) 5J; (e) intact specimens; (f) comparison of hysteresis energy densities per cycle at the edge of the specimens under different test conditions ($n = 500$ cycles).

carbon fibers), with cracks appearing on the back of the specimen, and carbon fibers breaking or delaminating in the CF/PEEK layer, leading to more dissipated energy per cycle.

4.2. Post-impact fatigue life prediction methodology

From the perspective of energy to analyze the fatigue of the laminate, the cyclic loading works on the specimen during fatigue, according to the first law of thermodynamics, this part of the energy will be converted into the following forms: the first part is the elastic strain energy, which is generated by the elastic deformation of the material and is recoverable after the cyclic loading of fatigue, producing no damage to the material; the second part is the plastic strain energy, which is the irrecoverable damage induced by the plastic deformation of the metal and polymer

layers; the third part is the energy dissipated by the formation of damage or fracture within the material, such as delamination, cracking of the metal and matrix, and breakage of fibers, as shown in Fig. 8; the last part is other forms of dissipated energy, as the result of internal friction, thermal energy is generated by the delamination or cracks within the material under the cyclic loading. Then, the energy during the entire course of fatigue satisfies:

$$W_T = W_E + W_P + W_D + W_Q \tag{3}$$

where, W_T, W_E, W_P, W_D, and W_Q are the work from external source, the elastic strain energy, the plastic strain energy, the damage dissipated energy, and the thermal energy, respectively.

In terms of energy density, Eq. (3) can be expressed as

$$w_T = w_E + w_P + w_D + w_Q \tag{4}$$

For a single cycle of fatigue, the elastic strain energy density is 0, and neither of the other three is 0. Therefore, the energy variations in the specimen system during a single cycle of fatigue and the full-life course can be simplified as Eqs. (5) and (6), which correspond to the area of the hysteresis loop enclosing the single cycle (the ith cycle) $\Delta w_{diss,i}$ (Fig. 10 (a)) and the sum of the areas of the hysteresis loop over the full-life course of fatigue w_{diss}, respectively.

$$\Delta w_{diss,i} = \Delta w_{P,i} + \Delta w_{D,i} + \Delta w_{Q,i} \tag{5}$$

$$w_{diss} = w_P + w_D + w_Q = \sum_{i=1}^{N} \Delta w_{diss,i} \tag{6}$$

where, N is the fatigue life.

The stress-strain relations under all cycles during fatigue testing are difficult to record completely. In this section, the DIC technique was used to capture the axial strain on the surface of specimen, and one full fatigue cycle was captured at an interval of 500 cycles as illustrated in Fig. 3(b).

Therefore, based on Eq. (6), the total dissipated energy density w_{diss} in the specimen system during fatigue can be approximately equivalent to the integral of the hysteresis energy density from the first cycle to fracture, that is

$$w_{diss} = \int_{1}^{N} \Delta w_{diss,i} dn \tag{7}$$

Since the fatigue phenomenon associated with fatigue life has an inherent power law nature [35], the dependence of the total dissipated energy density on the maximum stress and fatigue life can be fitted by the following equations in which α, β, η and γ are the model parameters.

$$w_{diss} = \alpha \sigma_{max}^{\beta} \tag{8}$$

$$w_{diss} = \eta N^{\gamma} \tag{9}$$

When the maximum stress remains constant during fatigue, increasing the stress amplitude ratio will narrow the stress history of the specimen and reduce the area of the hysteresis loop, indicating that the energy dissipated by a single cycle of fatigue is reduced, thus the fatigue life of the specimen is prolonged. It can be seen that the stress ratio is inversely related to the fatigue life. Therefore, when the maximum stress is constant (the total dissipated energy density in the specimen system is unchanged according to Eq. (8)), for the case where the stress ratio changes, a coefficient related to the stress ratio can be introduced on the basis of Eq. (9), which is noted as the coefficient of the stress ratio $\psi(R)$.

$$w_{diss} = \psi(R) \eta N^{\gamma} \tag{10}$$

Accordingly, $\psi(R)$ can be defined as the ratio of hysteresis energy density at the arbitrary stress ratio R (a quantity between 0 and 1) to the reference stress ratio R_0, which is

$$\psi(R) = \frac{\Delta w_{diss,i}(R)}{\Delta w_{diss,i}(R_0)} \tag{11}$$

To simplify the calculation, the area of the hysteresis loop is divided approximately into two triangles [42], as presented in Fig. 13. Thereinto, the bottom side of the triangle is the strain difference ε_m between the loading and unloading at the average stress, while the height of the triangle is the stress amplitude σ_a during fatigue, then the area of a single hysteresis loop can be expressed as

$$\Delta w_{diss} = \varepsilon_m \sigma_a = \left(\frac{1-R}{2}\right) \varepsilon_m \sigma_{max} \tag{12}$$

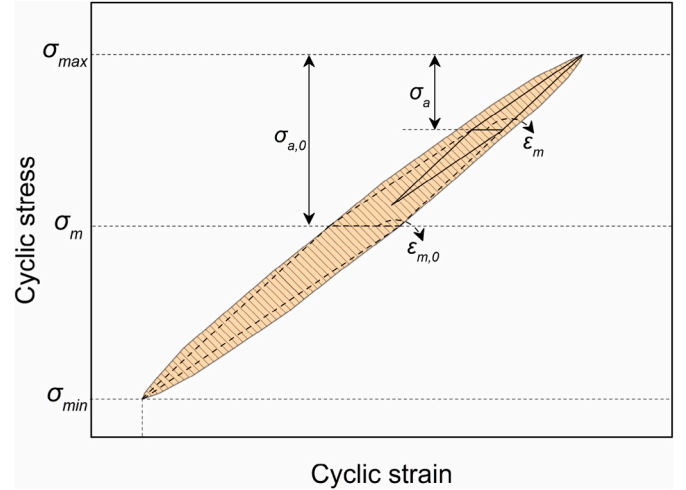By implementing Eq. (12) into Eq. (11) at the same maximum stress for two stress ratios,

Fig. 13. Equivalent schematic of hysteresis loop area.

$$\psi(R) = \frac{\varepsilon_m}{\varepsilon_{m,0}} \frac{1-R}{1-R_0} \tag{13}$$

According to the Thales's theorem, as depicted in Fig. 13, Eq. (13) can be simplified as

$$\psi(R) = \left(\frac{1-R}{1-R_0}\right)^2 \tag{14}$$

Substituting Eq. (10) into Eq. (8) yields the relation between the fatigue life and the stress ratio at a constant initial impact energy level:

$$\alpha \sigma_{max}^{\beta} = \psi(R) \eta N^{\gamma} \tag{15}$$

$$N = \left(\frac{\alpha}{\eta \psi(R)}\right)^{1/\gamma} (\sigma_{max})^{\beta/\gamma} \tag{16}$$

For the specimens impacted by various initial impact energy levels, the total dissipated energy density of the system is considered to be changed due to the change of the damage state within the laminate, thus a coefficient related to the initial impact energy level can be introduced based on Eq. (9), which is recorded as the impact damage coefficient $\Phi(E)$, as expressed in Eq. (17).

$$\Phi(E) w_{diss} = \eta N^{\gamma} \tag{17}$$

Similar to the coefficient of stress ratio, $\Phi(E)$ can be defined as the ratio of hysteresis energy density at the arbitrary impact energy level E to the reference impact energy level E_0, which is

$$\Phi(E) = \frac{\Delta w_{diss}(E)}{\Delta w_{diss}(E_0)} \tag{18}$$

The relation between the impact energy level and the total dissipated energy density of the laminate is defined as expressed in Eq. (19) in which A and B are model parameters related only to the maximum stress during fatigue:

$$w_{diss}(E) = A e^{B \cdot E} \tag{19}$$

The impact damage coefficient for constant maximum stress during fatigue can be simplified as

$$\Phi(E) = e^{B(E-E_0)} \tag{20}$$

Then, by substituting Eq. (17) into Eq. (8), the fatigue life of the specimen versus the initial impact energy level can be obtained when the stress ratio is constant:

$$\Phi(E) \alpha \sigma_{max}^{\beta} = \eta N^{\gamma} \tag{21}$$

$$N = \left(\frac{\Phi(E)\alpha}{\eta}\right)^{1/\gamma}(\sigma_{max})^{\beta/\gamma} \tag{22}$$

Therefore, combining Eqs. (16) and (22), the relation between the fatigue life and the stress ratio as well as the initial impact energy level while the maximum stress level remains constant during fatigue is derived as

$$N = \left(\frac{\Phi(E)\alpha}{\eta\psi(R)}\right)^{1/\gamma}(\sigma_{max})^{\beta/\gamma} \tag{23}$$

4.3. Determination of the parameters in the proposed model

The experimental data under the stress ratio of 0.1 and initial impact energy level of 20 J is used as input data to acquire the required model parameters (α, β, η, and γ) for predicting the post-impact fatigue life at other stress ratios. Firstly, the total dissipated energy density for the whole course of fatigue at an impact energy level of 20 J is available according to Eq. (7) and Fig. 12(a). Then, the evolution of the total dissipated energy density against the maximum stress and fatigue life in the double-logarithmic coordinate system can be plotted as shown in Fig. 14(a) and (b), respectively. It is observed that the total dissipated energy density decreases as the maximum stress increases. By fitting the experimental data using Eqs. (8) and (9), the model parameters are determined as presented in Fig. 14.

For the case of various initial impact energy levels, the parameters to be determined are A and B. According to Eq. (7) and Fig. 12(a–e), the total dissipated energy density of the intact and impacted specimen during the whole course of fatigue could be obtained, and then the evolution of the total dissipated energy with the level of impact energy at different maximum stress levels when the stress amplitude ratio is 0.1 is available as shown in Fig. 15. After preliminary fitting, it is found that B is essentially unaffected by changes in the maximum stress, which has a constant value (−0.06) over the range of maximum stress levels measured in the experiments (20%–50%), it can be assumed that B is a material-related parameter. Thus, changing the maximum stress level only has an effect on A. However, the impact damage coefficient $\Phi(E)$ is not affected by A from Eq. (20). It is then sufficient to require experimental data at only one maximum stress level to predict the residual fatigue life at other maximum stress levels.

4.4. Validation and analysis

The residual fatigue life of the specimens at various stress ratios and maximum stresses can be predicted by substituting the above-fitted model parameters (α, β, η, and γ) into Eq. (16) when the impact energy level is 20 J. As illustrated in Fig. 16(a), using the post-impact fatigue life distribution at the stress amplitude ratio of 0.1 as input data, the post-impact fatigue life of the laminate at various maximum stresses
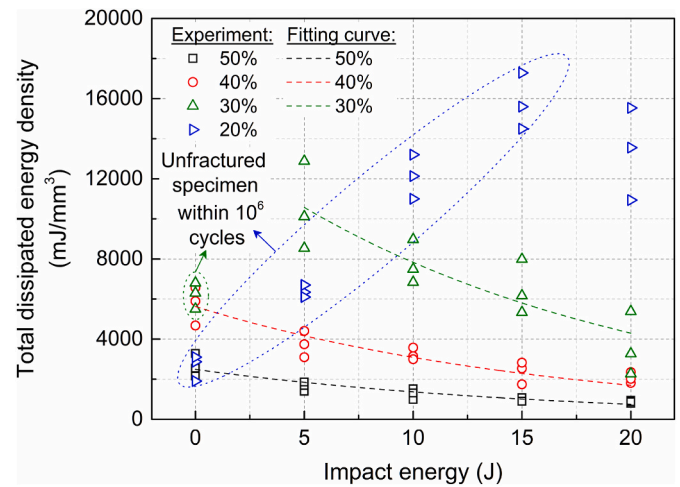

Fig. 15. Evolution of the total dissipated energy density of the specimens versus the impact energy levels at stress ratio 0.1 for different maximum stress levels.

is predicted when the stress amplitude ratios are 0.3 and 0.5, the maximum stress level (55%) beyond the fitted data is chosen for validation additionally. It is found that the predicted results of the proposed model are consistent with the trend of the experimental results. When the initial damage state of the specimen is the same (subjected to the same initial impact energy level), with the stress ratio increasing, the post-impact fatigue life of the specimen is increased under the same maximum stress, which is in accordance with the analysis of section 4.1. Furthermore, the comparison of the predicted fatigue lives with the experimental results at an initial impact energy level of 20 J is presented in Fig. 16(b), where it is observed that almost all the data points are distributed within the 2-scatter error bands, proving the satisfactory accuracy of the proposed model in predicting the residual fatigue life of the impacted specimens at various stress ratios and maximum stresses.

Moreover, the residual fatigue life of the specimens at various impact energy levels and maximum stresses when the stress ratio is 0.1 can be predicted as presented in Fig. 17(a) and (b) by substituting the fitted model parameters, which are α, β, η, γ, A and B. Since the residual fatigue life distribution at the impact energy levels of 5, 10, 15, and 20 J is used to determine the model parameter B in Eq. (20), the accuracy of the proposed model cannot be judged by using the impact energy levels involved in the model, thus, two additional impact energy levels not covered in the model are chosen to validate the proposed model, including one within the range of the fitted data (12.5 J) and one outside the range of the fitted data (25 J), while the maximum stress levels not involved in the model (35% and 45%) are selected for validation. The predicted and experimental results are shown in Fig. 17(b), it is found
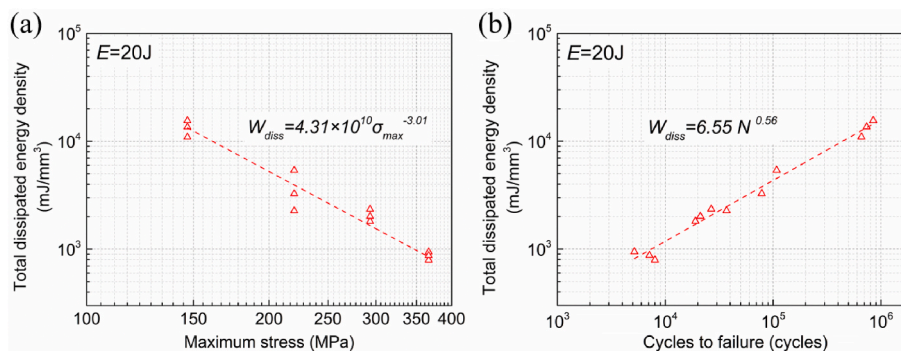

Fig. 14. For the specimens with the initial impact energy level of 20J at stress ratio 0.1: (a) evolution of the total dissipated energy versus the maximum stresses; (b) evolution of the total dissipated energy density versus the cycles to failure.
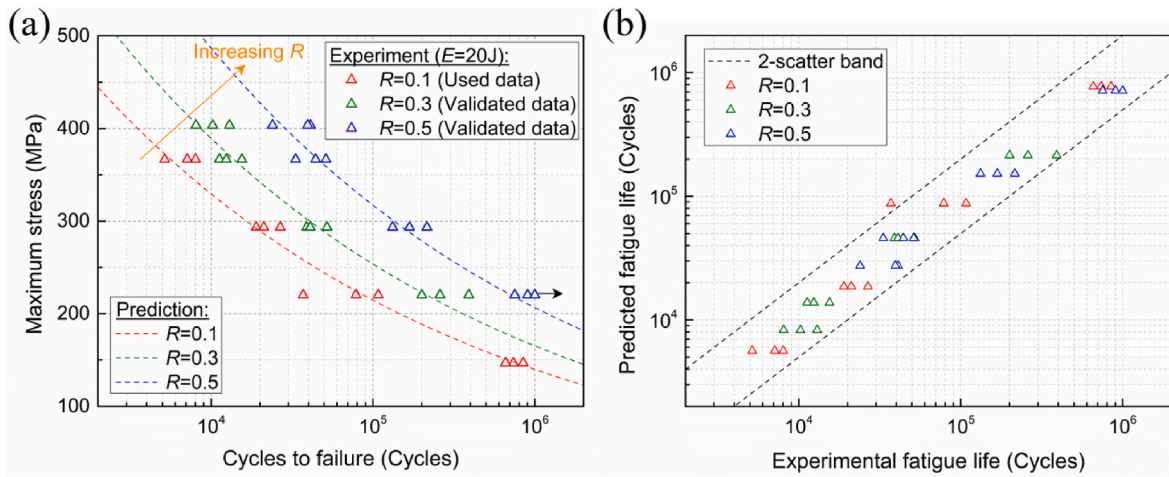
Fig. 16. (a) Residual fatigue life distribution of the specimens subjected to the initial impact energy level of 20J under various stress ratios and maximum stresses; (b) comparison of the predicted and experimental fatigue lives at the initial impact energy level of 20J.
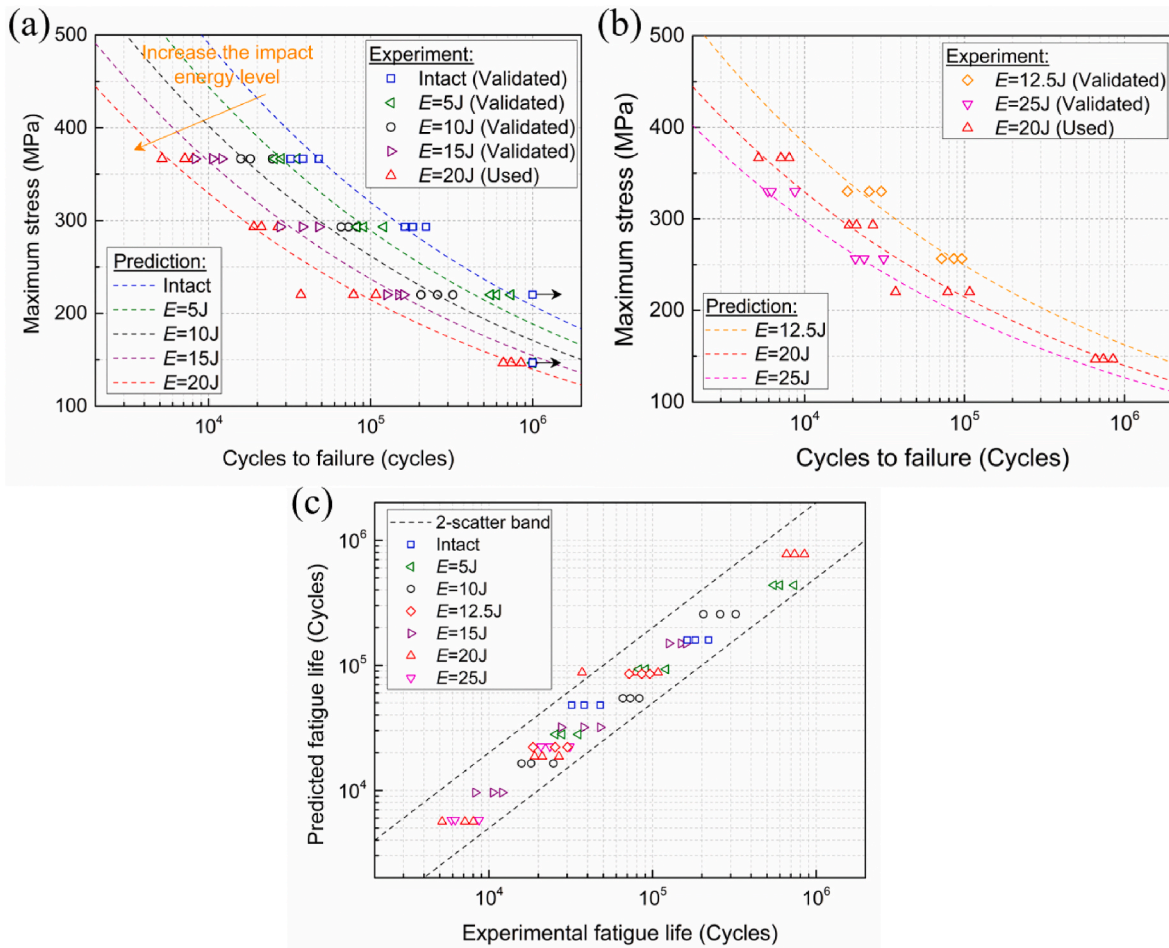

Fig. 17. Residual fatigue life distribution of the specimen with different initial impact energy levels under various maximum stresses at the stress ratio of 0.1: (a) experimental and predicted results covered in the proposed model; (b) experimental and predicted results not covered in the proposed model; (c) comparison of the predicted and experimental fatigue lives.

that the trend of the predicted results is consistent with that of the experiments, with the increase of the impact energy level, the post-impact fatigue life is gradually increased under the same maximum stress; meanwhile, under the same level of the impact energy, the post-impact fatigue life is gradually decreased with the increase of the maximum

stress. For all the predicted results at various impact energy levels, as shown in Fig. 17(c), most of the data points are located within the 2-scatter error band, proving the reliability of the proposed model.

In summary, the post-impact fatigue life prediction of CF/PEEK-Ti hybrid laminates with various stress ratios (tensile-tensile fatigue) and

initial impact energy levels (no penetration damage to the specimen) can be achieved by the proposed model, and the amount of required experiments as well as the cost is greatly reduced. It is worth mentioning that the model has only one material-related fitting parameter, which means that the model still has applicability for other kinds of FMLs (e.g., GLARE laminates).

5. Conclusions

In this study, for the specific service scenario of CF/PEEK-Ti hybrid laminates, the effects of different impact energy and maximum stress levels on the residual fatigue life of the laminates were investigated, the energy dissipation law of the laminates under different experimental conditions was analyzed, and based on the law, the post-impact fatigue life of the laminates is predicted for different stress ratios, impact energies and maximum stresses. The results show that the residual fatigue life of CF/PEEK-Ti hybrid laminates is substantially decreased by the impact damage, with the average residual fatigue life of the laminates decreasing to 17.2% of the average fatigue life of intact specimens when the maximum stress and the impact energy levels are 50% and 20 J, respectively. The axial strain distribution on the surface of the laminate is affected by the impact, leading to a stress concentration around the dent. The effects of impact damage on the residual fatigue life of laminates primarily consist of the localized stress concentration resulting from impact deformation, the delamination and breakage of fibers, and the amplification of the residual stress field by the dents. The proposed model can well predict the post-impact fatigue life of CF/PEEK-Ti hybrid laminates under different initial impact energies, maximum stresses and stress ratios, and by comparing the experimental results with other stress ratios and impact energies, the predicted results are distributed within the 2-scatter error bands and the reliability of the proposed method is proved. Meanwhile, the proposed model is also applicable to other types of FMLs (with only one material-related fitting parameter), and the post-impact fatigue life of the laminate can be accurately predicted with only one set of S–N curve data.

CRediT authorship contribution statement

Chunming Ji: Conceptualization, Methodology, Investigation, Data Curation, Writing - Original Draft, Writing - Review & Editing.
Jiqiang Hu: Formal analysis, Validation.
René Alderliesten: Methodology, Writing - Review & Editing.
Jinchuan Yang: Data Curation.
Zhengong Zhou: Writing - Review & Editing.
Yuguo Sun: Writing - Review & Editing.
Bing Wang: Supervision, Funding acquisition, Writing - Review & Editing.

Declaration of competing interest

The authors declare that they have no known competing financial interests or personal relationships that could have appeared to influence the work reported in this paper.

Data availability

Data will be made available on request.

Acknowledgement

References

[1] M. Sadighi, R.C. Alderliesten, R. Benedictus, Impact resistance of fiber-metal laminates: a review, Int. J. Impact Eng. 49 (2012) 77–90.
[2] Y. Chen, J. Yang, J. Peng, C. Ji, B. Wang, Low-velocity impact (LVI) and post-impact fatigue properties of GLARE laminates with holes, Int. J. Fatig. 167 (2023), 107318.
[3] Z.-Q. Cheng, W. Tan, J.-J. Xiong, E.-M. He, T.-H. Xiong, Y.-P. Wang, Modelling fatigue behaviours and lifetimes of novel GLARE laminates under random loading spectrum, Compos. Struct. 311 (2023), 116799.
[4] C. Ji, J. Hu, B. Wang, Y. Zou, Y. Yang, Y. Sun, Mechanical behavior prediction of CF/PEEK-titanium hybrid laminates considering temperature effect by artificial neural network, Compos. Struct. 262 (2020), 113367.
[5] J. Zhang, Q. Qin, J. Zhang, H. Yuan, J. Du, H. Li, Low-velocity impact on square sandwich plates with fibre-metal laminate face-sheets: analytical and numerical research, Compos. Struct. 259 (2021), 113461.
[6] N.R.J. Hynes, N.J. Vignesh, J.T.W. Jappes, P.S. Velu, C. Barile, M.A. Ali, et al., Effect of stacking sequence of fibre metal laminates with carbon fibre reinforced composites on mechanical attributes: numerical simulations and experimental validation, Compos. Sci. Technol. 221 (2022), 109303.
[7] J. Edwin Raja Dhas, M. Arun, A review on development of hybrid composites for aerospace applications, Mater. Today Proc. 64 (2022) 267–273.
[8] Y. Chen, J. Yang, X. Qiu, C. Ji, B. Wang, DIC-based constant amplitude and two-block loading fatigue life prediction of open hole GLARE laminate, Eng. Fract. Mech. 278 (2023), 109016.
[9] D.A. Burianek, S.M. Spearing, Fatigue damage in titanium-graphite hybrid laminates, Compos. Sci. Technol. 62 (2002) 607–617.
[10] Y. Hu, Y. Zhang, X. Fu, G. Hao, W. Jiang, Mechanical properties of Ti/CF/PMR polyimide fiber metal laminates with various layup configurations, Compos. Struct. 229 (2019), 111408.
[11] C. Ji, B. Wang, J. Hu, C. Zhang, Y. Sun, Effect of different preparation methods on mechanical behaviors of carbon fiber-reinforced PEEK-Titanium hybrid laminates, Polym. Test. 85 (2020), 106462.
[12] Y. Chen, C. Ji, X. Pan, J. Yang, B. Wang, Effect of staggered holes with multi-site damage on fatigue performance based on tests, DIC technique and numerical calculations, Thin-Walled Struct. 148 (2020), 106607.
[13] J. Zhang, Y. Ye, Q. Qin, T. Wang, Low-velocity impact of sandwich beams with fibre-metal laminate face-sheets, Compos. Sci. Technol. 168 (2018) 152–159.
[14] J.O. Peters, R.O. Ritchie, Influence of foreign-object damage on crack initiation and early crack growth during high-cycle fatigue of Ti-6Al-4V, Eng. Fract. Mech. 67 (2000) 193–207.
[15] J. Zhang, Y. Zhu, K. Li, H. Yuan, J. Du, Q. Qin, Dynamic response of sandwich plates with GLARE face-sheets and honeycomb core under metal foam projectile impact: experimental and numerical investigations, Int. J. Impact Eng. 164 (2022), 104201.
[16] Y. Chen, C. Ji, C. Zhang, F. Wang, X. Song, Analysis for post-impact tensile-tensile fatigue damage of 2024-T3 sheets based on tests, digital image correlation (DIC) technique and finite element simulation, Int. J. Fatig. 122 (2019) 125–140.
[17] Y. Chen, X. Pan, C. Zhang, Z. Cui, C. Ji, Influence of foreign object impact mode on fatigue performance of 2198-T8 Al-Li alloy thin sheets for fuselage, Fatig. Fract. Eng. Mater. Struct. 44 (2021) 115–128.
[18] Z. Li, R. Feng, Y. Wang, L. Wang, Experimental study on the effect of dents induced by impact on the fatigue life of 2024-T3 aluminum alloy plate, Eng. Struct. 137 (2017) 236–244.
[19] Z. Li, D. Zhang, C. Peng, C. Ma, J. Zhang, Z. Hu, et al., The effect of local dents on the residual ultimate strength of 2024-T3 aluminum alloy plate used in aircraft under axial tension tests, Eng. Fail. Anal. 48 (2015) 21–29.
[20] H. Ma, K. Lu, X. Liu, Experimental and numerical studies on lateral low-velocity impact behaviour and residual axial strength of circular aluminum alloy (6061-T6) tubes, Structures 47 (2023) 1250–1264.
[21] Z. Li, M. Zhang, F. Liu, C. Ma, J. Zhang, Z. Hu, et al., Influence of dent on residual ultimate strength of 2024-T3 aluminum alloy plate under axial compression, T. Nonferr. Metal. Soc. 24 (10) (2014) 3084–3094.
[22] C. Ji, Y. Chen, J. Yang, B. Wang, Y. Sun, Dent-repaired fatigue performance and life prediction of thin sheet specimens under coupled multi-stage damage with impact and pre-fatigue, Int. J. Fatig. 146 (2021), 106148.
[23] N.J. Orchowski, R.D. Mohammed, G. Clark, M. Brandt, The post-repair performance of Ti-6Al-4V after foreign object damage, Proc. Eng. 10 (2011) 3622–3627.
[24] J.F. Laliberté, C. Poon, P.V. Straznicky, A. Fahr, Post-impact fatigue damage growth in fiber-metal laminates, Int. J. Fatig. 24 (2002) 249–256.
[25] H. Seo, H.T. Hahn, J.-M. Yang, Impact damage tolerance and fatigue durability of GLARE lamiantes, J. Eng. Mater.-T. ASME 130 (2008), 041002.
[26] R. Bogenfeld, P. Schmiedel, N. Kuruvadi, T. Wille, J. Kreikemeier, An experimental study of the damage growth in composite laminates under tension-fatigue after impact, Compos. Sci. Technol. 191 (2020), 108082.
[27] P. Alam, D. Mamalis, C. Robert, C. Floreani, C.M. Ó Brádaigh, The fatigue of carbon fibre reinforced plastics - a review, Compos. Part B-Eng. 166 (2019) 555–579.
[28] D.U. Shah, P.J. Schubel, M.J. Clifford, P. Licence, Fatigue life evaluation of aligned plant fibre composites through S–N curves and constant-life diagrams, Compos. Sci. Technol. 74 (2013) 139–149.
[29] I. Ben-Yelun, M. Díaz-Lago, L. Saucedo-Mora, M.Á. Sanz, R. Callado, F.J. Montáns, Self-learning locally-optimal hypertuning using maximum entropy, and comparison of machine learning approaches for estimating fatigue life in composite materials of the aerospace industry, Eng. Struct. 283 (2023), 115829.

[30] W.X. Yao, N. Himmel, A new cumulative fatigue damage model for fibre-reinforced plastics, Compos. Sci. Technol. 60 (2000) 59–64.

[31] W. Van Paepegem, J. Degrieck, A new coupled approach of residual stiffness and strength for fatigue of fibre-reinforced composites, Int. J. Fatig. 24 (2002) 747–762.

[32] J.-M. Koo, J.-H. Choi, C.-S. Seok, Evaluation for residual strength and fatigue characteristics after impact in CFRP composites, Compos. Struct. 105 (2013) 58–65.

[33] R. Talreja, Damage and fatigue in composites - a personal account, Compos. Sci. Technol. 68 (13) (2008) 2585–2591.

[34] V.A. Passipoularidis, T.P. Philippidis, P. Brondsted, Fatigue life prediction in composites using progressive damage modelling under block and spectrum loading, Int. J. Fatig. 33 (2) (2011) 132–144.

[35] A.V. Movahedi-Rad, G. Eslami, T. Keller, A novel fatigue life prediction methodology based on energy dissipation in viscoelastic materials, Int. J. Fatig. 152 (2021), 106457.

[36] A. Li, J. Huang, C. Zhang, Enabling rapid fatigue life prediction of short carbon fiber reinforced polyether-ether-ketone using a novel energy dissipation-based model, Compos. Struct. 272 (2021), 114227.

[37] C. Ji, J. Guo, J. Hu, B. Wang, Y. Sun, Enhanced interfacial adhesion of CF/PEEK-titanium hybrid laminates via introducing micro-nano layers with multi-walled carbon nanotube networks, Compos. Sci. Technol. 223 (2022), 109418.

[38] C. Ji, J. Hu, M. Sadighi, R. Alderliesten, B. Wang, Y. Sun, Experimental and theoretical study on residual ultimate strength after impact of CF/PEEK-titanium hybrid laminates with nano-interfacial enhancement, Compos. Sci. Technol. 232 (2023), 109871.

[39] I. De Baere, W. Van Paepegem, M. Quaresimin, J. Degrieck, On the tension-tension fatigue behaviour of a carbon reinforced thermoplastic part I: limitations of the ASTM D3039/D3479 standard, Polym. Test. 30 (6) (2011) 625–632.

[40] Y. Zhao, R. Alderliesten, Z. Zhou, G. Fang, J. Zhang, R. Benedictus, On the physics of applying finite width and geometry correction factors in fatigue crack growth predictions of GLARE, Int. J. Fatig. 117 (2018) 189–195.

[41] P. Zhu, J. Lin, R. Xiao, H. Zhou, Unravelling physical origin of the Bauschinger effect in glassy polymers, J. Mech. Phys. Solid. 168 (2022), 105046.

[42] H.T. Hann, R.Y. Kim, Fatigue behavior of composite laminate, J. Compos. Mater. 10 (2) (1976) 156–180.